

2003

Compact Supercell Method Based on Opposite Parity for Bragg Fibers

Wang Zhi

Ren Guobin

Lou Shuquin

Liang Weijun

Shangping Guo
Old Dominion University

Follow this and additional works at: https://digitalcommons.odu.edu/ece_fac_pubs

 Part of the [Bioimaging and Biomedical Optics Commons](#), [Electrical and Computer Engineering Commons](#), and the [Optics Commons](#)

Repository Citation

Zhi, Wang; Guobin, Ren; Shuquin, Lou; Weijun, Liang; and Guo, Shangping, "Compact Supercell Method Based on Opposite Parity for Bragg Fibers" (2003). *Electrical & Computer Engineering Faculty Publications*. 62.
https://digitalcommons.odu.edu/ece_fac_pubs/62

Original Publication Citation

Wang, Z., Ren, G.B., Lou, S.Q., Liang, W.J., & Guo, S.P. (2003). Compact supercell method based on opposite parity for Bragg fibers. *Optics Express*, 11(26), 3542-3549. doi: 10.1364/oe.11.003542

Compact supercell method based on opposite parity for Bragg fibers

Wang Zhi, Ren Guobin, Lou Shuqin, Liang Weijun

Institute of Lightwave Technology, Beijing Jiaotong University, Beijing 100044
zhiwang@center.njtu.edu.cn

Shangping Guo

Photonics Laboratory, Department of Electrical & Computer Engineering
Old Dominion University, Virginia, 23529
sguox002@odu.edu

Abstract: The supercell-based orthonormal basis method is proposed to investigate the modal properties of the Bragg fibers. A square lattice is constructed by the whole Bragg fiber which is considered as a supercell, and the periodical dielectric structure of the square lattice is decomposed using periodic functions (cosine). The modal electric field is expanded as the sum of the orthonormal set of Hermite-Gaussian basis functions based on the opposite parity of the transverse electric field. The propagation characteristics of Bragg fibers can be obtained after recasting the wave equation into an eigenvalue system. This method is implemented with very high efficiency and accuracy.

©2003 Optical Society of America

OCIS codes: (060.2280) Fiber design and fabrication, (060.2310) Fiber optics, (230.7370) Waveguides

References and links

1. P.Yeh, A. Yariv, E. Marom, "Theory of Bragg fibers," *J. Opt. Soc. Am.*, **68**, 1196-1201(1978).
2. Y.Fink, J.N. Winn, S.H. Fan, C.Chen, J. Michel, J.D. Joannopoulos, E.L. Thomas, "A dielectric omnidirectional reflector," *Science* **282**, 1679-1682(1998).
3. Y.Fink, D.J. Ripin, S.Fan, C. Chen, J.D. Joannopoulos, E.L. Thomas, "Guiding optical light in air using an all-dielectric structure," *J. Lightwave Technol.* **17**, 2039-2041 (1999).
4. M.Ibanescu, Y.Fink, S.Fan, E.L. Thomas, J.D. Joannopoulos, "An all-dielectric coaxial waveguide," *Science* **289**, 415-419(2000).
5. S.D. Hart, G.R.Maskaly, B.Temelkuran, P.H. Pridaux, J.D. Joannopoulos, Y.Fink, "External reflection from omnidirectional dielectric mirror fibers," *Science* **296**, 510-513(2002).
6. P. Russell, "Photonic crystal fibers," *Science* **299**, 358-362 (2003).
7. J.C. Knight, P. St. Russell, "New ways to guide light," *Science* **296**, 276-277 (2002).
8. Jes Broeng, Stig E. B. Libori, T. Sondergaard, and Anders Bjarklev, "Analysis of air-guiding photonic bandgap fibers," *Opt. Lett.* **25**, 96-98 (2000).
9. M. Ibanescu, S.G. Johnson, M. Soljacic, J.D. Joannopoulos, Y.Fink, "Analysis of mode structure in hollow dielectric waveguide fibers," *Phys. Rev. E* **67**, 046608-1-8(2003).
10. I.M. Bassett, A. Argyros, "Elimination of polarization degeneracy in round waveguides," *Opt. Express* **10**, 1342-1346 (2002), <http://www.opticsexpress.org/abstract.cfm?URI=OPEX-10-23-1342>.
11. S.G. Johnson, M. Ibanescu, M. Skorobogatiy, O. Weisberg, T.D. Engeness, M. Soljacic, S.A. Jacobs, J.D. Joannopoulos, Y.Fink, "Low-loss asymptotically single-mode propagation in large-core omniguide fibers," *Opt. Express* **9**, 748-779 (2001), <http://www.opticsexpress.org/abstract.cfm?URI=OPEX-9-13-748>.
12. G. Ourang, Yong Xu, A. Yariv, "Theoretical study on dispersion compensation in air-core Bragg fibers," *Opt. Express* **10**, 899-908 (2002), <http://www.opticsexpress.org/abstract.cfm?URI=OPEX-10-17-899>.
13. T.D. Engeness, M. Ibanescu, S.G. Johnson, O.Weisberg, M.Skorobogatiy, S.Jacobs, Y.Fink, "Dispersion tailoring and compensation by modal interactions in omniguide fibers," *Opt. Express* **11**, 1175-1196 (2003), <http://www.opticsexpress.org/abstract.cfm?URI=OPEX-11-10-1175>.
14. J.A.Mosoriu, E. Silvestre, A. Ferrando, P.Andres, J.J. Miret, "High-index-core Bragg fibers: dispersion properties," *Opt. Express* **11**, 1400-1405 (2003), <http://www.opticsexpress.org/abstract.cfm?URI=OPEX-11-12-1400>.

15. E. Silvestre, M.V. Andrés, and P. Andrés, "Biorthonormal-basis method for the vector description of optical-fiber mode," *J. Lightwave Technol.* **16**, 923-928 (1998).
16. R. D. Meade, A.M. Rappe, K.D. Brommer, J.D. Joannopoulos, and O.L. Alerhand, "Accurate theoretical analysis of photonic band-gap materials," *Phys. Rev. B* **48**, 8434-8437 (1993).
17. Shangping Guo, Feng Wu, Khalid Ikram, and Sacharia Albin, "Analysis of circular fibers with arbitrary index profile by Galerkin method," to be published by *Opt. Lett.*
18. J.D. Joannopoulos, R.D. Meade, J.N. Winn, "Photonic crystals: molding the flow of light," (New York, Princeton university press, 1995).
19. Shangping Guo, Sacharia Albin, "Simple plane wave implementation for photonic crystal calculations," *Opt. Express* **11**, 167-175 (2003), <http://www.opticsexpress.org/abstract.cfm?URI=OPEX-11-2-167>.
20. A.W. Snyder, J.D. Love, *Optical waveguide theory*, (New York: Chapman and Hall, 1983).
21. T.M. Monro, D.J. Richardson, N.G.R. Broderick, P.J. Bennett, "Holey optical fibers: an efficient modal model," *J. Lightwave Technol.* **17**, 1093-1102 (1999).
22. Yu-Li Hsueh, E. S.T. Hu, M. E. Marhic, . G. Kazovsky, "Opposite-parity orthonormal function expansion for efficient full-vectorial modeling of holey optical fibers," *Opt. Lett.* **28**, 1188-1190(2003).
23. W. Zhi, R.G. Bin, L.S. Qin, and J.S.Sheng, "Supercell lattice method for photonic crystal fibers," *Opt. Express* **11**, 980-991 (2003), <http://www.opticsexpress.org/abstract.cfm?URI=OPEX-11-9-980>.
24. R.G. Bin, W. Zhi, L.S. Qin, J.S. Sheng, "Mode Classification and Degeneracy in Photonic Crystal Fiber," *Opt. Express* **11**, 1310-1321 (2003), <http://www.opticsexpress.org/abstract.cfm?URI=OPEX-11-11-1310>.

1. Introduction

At the beginning of the optical fiber progress, the ring fiber had been investigated by the transfer matrix method [1]. There was not much more attention paid to it because the index difference between every layer was very small. The ring fibers have attracted much interest because of their extraordinary properties when the great index difference dielectric materials were used at the end of last century [2-5]. The ring fiber has some new names called "Coaxial fiber", "Omniguide fiber", or "Bragg fiber", in which the guiding of the light in the low-index core is due to the photonic band gap (PBG) produced by the periodic cladding, instead of the total internal reflection (TIR).

In the conventional metallic coaxial cable, the entire electromagnetic field is confined between two coaxial metal cylinders. The fundamental electromagnetic mode of a coaxial cable is the transverse electromagnetic (TEM) mode, which has radial symmetry in the electric field distribution and a linear relationship between frequency and wave vector.

Optical waveguide is restricted to the use of dielectric materials at optical wavelengths because of heavy absorption losses in the metal. However, because of the differences in boundary conditions of the electromagnetic fields at metal and dielectric surfaces, it has not previously been possible to recreate a TEM-like mode with all-dielectric materials. Consequently, optical waveguiding is done with the traditional total internal reflection (TIR) mechanism, by which the waveguides can achieve very low losses.

Recently, all-dielectric waveguides have been introduced that confine optical light by means of 1D or 2D photonic band gap [6-8]. These new designs have the potential advantage that light propagates mainly through the empty core of a hollow waveguide, thus minimizing effects associated with material nonlinearities, absorption losses and sharp bending.

The coaxial omniguide Bragg fiber, which combines some of the best features of the metallic coaxial cable and the dielectric waveguides, is an all-dielectric coaxial waveguide and supports a truly single mode in a low-index air core, which is very similar to the TEM mode of the metallic coaxial cable [2-5]. It has a radially symmetric electric field distribution so that the polarization is maintained throughout propagation [4,9-11]. It can be designed to be single-mode over a wide range of frequencies [11]. In addition, the mode has a point of intrinsic zero dispersion around which a pulse can retain its shape during propagation [12-14]. Finally, the coaxial omniguide can be used to guide light around sharp bends whose radius of curvature can be as small as the wavelength of the light [4,5].

There are a few different approaches to calculate the modes of the Bragg fibers, such as the semi-analytic approach based on the transfer matrix method [1], the asymptotic matrix method [11,12], the bi-orthonormal-basis method [14,15], and the approach involving a

numerical solution of Maxwell's equations in the frequency domain with the use of the conjugate gradient method within the supercell approximation [16]. The most recent Galerkin method [17] can be used to analyze the circular fibers with arbitrary index profile.

The supercell-based orthonormal basis method is proposed in this article. In section 2, the square lattice of the dielectric structure is constructed by arranging the whole Bragg fiber along x - and y - direction. In Section 3, the transverse electric field is decomposed into Hermite-Gaussian basis based on the opposite parity of the transverse electric field, and an eigenvalue system is deduced from the full-vectorial coupling wave equations. In Section 4, a Bragg fiber, which has the same structure as in Ref. [11], is considered as an example, and the numerical results agree with it. Section 5 is the conclusion.

2. Supercell of the dielectric structure

The air-guiding Bragg fiber is a cylindrical multilayered fiber, which is a cylindrically symmetric microstructured fiber having a hollow core surrounded by a multilayered cladding made of alternating layers of a higher and a lower refractive-index dielectric. The multilayered structure geometry is characterized by the radial multiplayer period, A , and the low-index-layer thickness, a , as illustrated in Fig. 1(a). The dielectric constants are alternately ϵ_1 and ϵ_2 , where $\epsilon_2 < \epsilon_1$. The dielectric constant of the hollow core is ϵ_3 , and its radius is R . In order to analyze this fiber, a square lattice is constructed by the whole transverse profile of the Bragg fiber that is considered as a supercell, the lattice constant of the square lattice is D , as illustrated in Fig. 1(b).

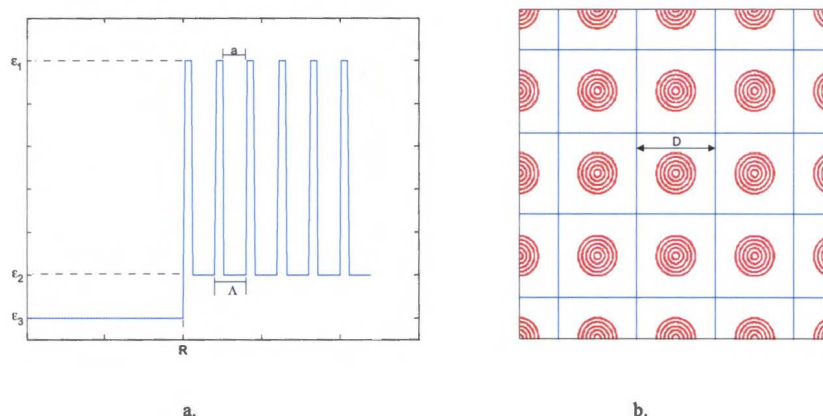


Fig. 1. scheme of the construction of the supercell square lattice of the Bragg fiber, (a) is the radial distribution of the dielectric constant and (b) is the supercell square lattice.

The periodic dielectric constant structure should be transferred into its Fourier transform when one is investigating photonic crystals, photonic crystal fibers or Bragg fibers [18,19], then the wave equation will be solved with the Fourier transform. For the supercell with length D in Fig. 1(b), the Fourier transform of the dielectric constant is:

$$\epsilon_F(\mathbf{k}) = \frac{1}{A} \iint_A \epsilon(\mathbf{r}) e^{-i\mathbf{k}\cdot\mathbf{r}} ds, \quad (1)$$

where $\mathbf{r}=(x, y)$ is the space position, $A=D^2$ is the area of the supercell, $\mathbf{k}=(k_x, k_y)$, the vector in the reciprocal space of the supercell lattice, is linearly combined by the primitive reciprocal lattice vectors $(2\pi/D, 2\pi/D)$, $\epsilon(\mathbf{r})$ is the dielectric structure of the supercell, which can be expressed in different regions as follows:

$$\epsilon(\mathbf{r}) = \begin{cases} \epsilon_i, & r_{i-1} < r < r_i \\ \epsilon_b, & r > r_m \end{cases} = \epsilon_b + \begin{cases} \epsilon_i - \epsilon_b, & r_{i-1} < r < r_i \\ 0, & r > r_m \end{cases}, \quad (2)$$

where ϵ_i and r_i are the dielectric constant and the outer radius of the i th layer, and r_0 is set zero, m is the total number of the layers, ϵ_b is the background dielectric constant. Eq. (1) will be analytically expressed as [18]:

$$\begin{aligned} \epsilon_F(\mathbf{k}) &= \frac{1}{A} \iint_A \epsilon_b e^{-i\mathbf{k}\cdot\mathbf{r}} ds + \frac{1}{A} \sum_{i=1}^m \iint_A (\epsilon_i - \epsilon_b) e^{-i\mathbf{k}\cdot\mathbf{r}} ds \\ &= \epsilon_b \delta(k) + \sum_{i=1}^m (\epsilon_i - \epsilon_b) \left[\frac{2f_i J_1(kr_i)}{kr_i} - \frac{2f_{i-1} J_1(kr_{i-1})}{kr_{i-1}} \right], \end{aligned} \quad (3)$$

where $k=|\mathbf{k}|$, $f_i=\pi r_i^2/A$ is the filling ratio. The limitation will be used when $k=0$ in Eq. (3).

Because the dielectric constant structure of the Bragg fiber has the x - and y - axial symmetric, i.e., $\epsilon(-x,y)=\epsilon(x,y)=\epsilon(x,-y)$, it can be expressed as a sum of the cosine functions as

$$\begin{aligned} \epsilon(\mathbf{r}) = \epsilon(x, y) &= \sum_{a,b=0}^P P_{ab} \cos \frac{2\pi ax}{D} \cos \frac{2\pi by}{D} \\ \ln \epsilon(\mathbf{r}) = \ln \epsilon(x, y) &= \sum_{a,b=0}^P P_{ab}^{\ln} \cos \frac{2\pi ax}{D} \cos \frac{2\pi by}{D}, \end{aligned} \quad (4)$$

where $(P+1)$ is the number of the expansion items, P_{ab} , P_{ab}^{\ln} are the expansion coefficients which can be analytically evaluated from the Fourier transform $\epsilon_F(\mathbf{k})$ in Eq. (3) and expressed as Eq. (5).

$$P_{ab} = \epsilon_F(\mathbf{k}_{a+P,b+P}) + \epsilon_F(\mathbf{k}_{a+P,-b+P}) + \epsilon_F(\mathbf{k}_{-a+P,b+P}) + \epsilon_F(\mathbf{k}_{-a+P,-b+P}), \quad (5a)$$

$$\text{for } a=0 \text{ or } b=0, P_{ab} = \epsilon_F(\mathbf{k}_{a+P,b+P}) + \epsilon_F(\mathbf{k}_{a+P,-b+P}), \quad (5b)$$

$$\text{for } a=0 \text{ and } b=0, P_{00} = \epsilon_F(\mathbf{k}_{P,P}), \quad (5c)$$

where $\mathbf{k}_{m,n}=(k_x, k_y)=2\pi D \times (m, n)$. P_{ab}^{\ln} can also be analytically evaluated from the Fourier transform of the logarithm of the dielectric constant distribution $\ln \epsilon(\mathbf{r})$.

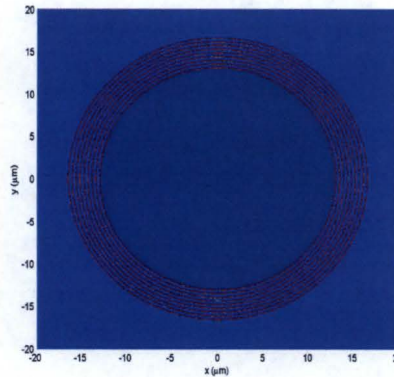


Fig. 2. The simulation result of the dielectric constant of the Bragg fiber, with the parameters $\epsilon_1=4.6^2$, $\epsilon_2=1.6^2$, $\epsilon_3=1.0$, $A=0.434\mu\text{m}$, $R=30A$, $\alpha=0.78A$, and $m=17$, supercell lattice constant $D=1.2(2R+18A)$, $P=1200$.

Figure 2 is the simulation result of the dielectric constant structure of the Bragg fiber, which has the same structure parameters as the Fig. 4 in Ref. [11]. The central area is the air-core with radius $R=30A$, and $A=0.434\mu\text{m}$. The dielectric constant of the periodical cladding are $\epsilon_1=4.6^2$ and $\epsilon_2=1.6^2$, the background is ϵ_2 too. There are 17 layers, and the lower-index layer thickness is $a=0.78A$. The supercell lattice constant D is set as $1.2(2R+18A)$, the expansion parameter $P=1200$.

3. Eigenvalue system

3.1 opposite parity of the mode field

When the confinement loss and the absorption loss are ignored in a normal waveguide which is uniform along the longitudinal direction (z -axis), both components $e_x(x,y)$ and $e_y(x,y)$ of the transverse electric field must satisfy the full-vectorial coupling wave equations [20,21]:

$$\begin{aligned} (\nabla_t^2 - \beta^2 + k_0^2 \epsilon) e_x &= -\frac{\partial}{\partial x} \left(e_x \frac{\partial \ln \epsilon}{\partial x} + e_y \frac{\partial \ln \epsilon}{\partial y} \right) \\ (\nabla_t^2 - \beta^2 + k_0^2 \epsilon) e_y &= -\frac{\partial}{\partial y} \left(e_x \frac{\partial \ln \epsilon}{\partial x} + e_y \frac{\partial \ln \epsilon}{\partial y} \right) \end{aligned} \quad (6)$$

where β is the propagation constant corresponding to the mode field distribution (e_x, e_y), $k_0=2\pi/\lambda$ is the wave number of the vacuum.

When $e(x, y)$ is an even function about both the x and y directions, it can be proved that $e_x(x,y)$ and $e_y(x,y)$ always have opposite parities in the x and y directions for each guided eigenmode [22]. It is also to say that, when one transverse component is an even function about one axis, the other will be an odd function about the same axis. For example, if $e_x(x,y)$ is an even function about x , $e_y(x,y)$ will be an odd function about x , i.e., $e_x(-x,y)=e_x(x,y)$, $e_y(-x,y)=-e_y(x,y)$.

3.2 subscripts

For the case of compactness, two subscripts m and n are introduced to express the opposite parity of the mode electric field, which have the logical value 0 or 1, and are used to describe the symmetry of the x -component $e_x(x,y)$ as $e_x(-x,y)=(-1)^m e_x(x,y)$ and $e_x(x,-y)=(-1)^n e_x(x,y)$. All the compositions of 'mn' are [00, 01, 10, 11], which can completely express the symmetry of the mode electric field about both axes. For example, the subscript '10' means that $e_x(x,y)$ is an odd function about x and an even function about y , $e_y(x,y)$ is an even function about x and an odd function about y .

In order to obtain the characteristics of the modes in the Bragg fibers, the transverse electric field can be expanded using the localized orthonormal Hermite-Gaussian basis functions as follows based on the opposite parity of the electric field.

$$e_x(x, y)_{mn} = \sum_{a,b=0}^{F-1} \mathcal{E}_{ab}^x \psi_{2a+m}(x) \psi_{2b+n}(y), \quad e_y(x, y)_{\bar{m}\bar{n}} = \sum_{a,b=0}^{F-1} \mathcal{E}_{ab}^y \psi_{2a+\bar{m}}(x) \psi_{2b+\bar{n}}(y), \quad (7)$$

where the bar over the subscript means the logical operator 'NOT', and the subscript 'mn' means that there are four sets of (e_x, e_y) with different parity. In Eq. (7), F is the number of the expansion terms, \mathcal{E}_{ab}^s ($s=x,y$) are the expansion coefficients, $\psi_i(s)$ is the i th order orthonormal Hermite-Gaussian function which is defined as:

$$\psi_i(s) = \frac{2^{-i/2} \pi^{-1/4}}{\sqrt{i! \omega_s}} \exp\left(-\frac{s^2}{2\omega_s^2}\right) H_i(s/\omega_s), \quad (8)$$

where $H_i(s/\omega_s)$ is the i th Hermite function which has the parity of $H_i(-s/\omega_s)=(-1)^i H_i(s/\omega_s)$, ω_s is the character width [21,22].

3.3 eigen equations

Substituting the decomposition equations of the dielectric constant and the field Eqs. (4) and (7) into Eq. (6), four sets of eigen equations will be obtained and shown in Eq. (9).

$$L_{mn} \begin{bmatrix} \mathcal{E}^x \\ \mathcal{E}^y \end{bmatrix} \equiv \begin{bmatrix} [I_{abcd}^{(1)} + k^2 I_{abcd}^{(2)} + I_{abcd}^{(3)x}]_{mn} & [I_{abcd}^{(4)x}]_{mn} \\ [I_{abcd}^{(4)y}]_{mn} & [I_{abcd}^{(1)} + k^2 I_{abcd}^{(2)} + I_{abcd}^{(3)y}]_{mn} \end{bmatrix} \begin{bmatrix} \mathcal{E}^x \\ \mathcal{E}^y \end{bmatrix} = \beta^2 \begin{bmatrix} \mathcal{E}^x \\ \mathcal{E}^y \end{bmatrix}, \quad (9)$$

where L_{mn} is a four-dimensional matrix, $I^{(1)}$, $I^{(2)}$, $I^{(3)}$ and $I^{(4)}$ are the overlapping integrals which are four-dimensional $F \times F \times F \times F$ matrix and expressed as follows.

$$[I_{abcd}^{(1)}]_{mn} = \int \int_{-\infty}^{+\infty} \psi_{2a+m}(x) \psi_{2b+n}(y) \nabla_t^2 [\psi_{2c+m}(x) \psi_{2d+n}(y)] dx dy, \quad (10.a)$$

$$[I_{abcd}^{(2)}]_{mn} = \int \int_{-\infty}^{+\infty} \epsilon \psi_{2a+m}(x) \psi_{2b+n}(y) \psi_{2c+m}(x) \psi_{2d+n}(y) dx dy, \quad (10.b)$$

$$[I_{abcd}^{(3)x}]_{mn} = \int \int_{-\infty}^{+\infty} \psi_{2a+m}(x) \psi_{2b+n}(y) \frac{\partial}{\partial x} \left[\psi_{2c+m}(x) \psi_{2d+n}(y) \frac{\partial \ln \epsilon}{\partial x} \right] dx dy, \quad (10.c)$$

$$[I_{abcd}^{(3)y}]_{mn} = \int \int_{-\infty}^{+\infty} \psi_{2a+m}(x) \psi_{2b+n}(y) \frac{\partial}{\partial y} \left[\psi_{2c+m}(x) \psi_{2d+n}(y) \frac{\partial \ln \epsilon}{\partial y} \right] dx dy, \quad (10.d)$$

$$[I_{abcd}^{(4)x}]_{mn} = \int \int_{-\infty}^{+\infty} \psi_{2a+m}(x) \psi_{2b+n}(y) \frac{\partial}{\partial x} \left[\psi_{2c+m}(x) \psi_{2d+n}(y) \frac{\partial \ln \epsilon}{\partial y} \right] dx dy, \quad (10.e)$$

$$[I_{abcd}^{(4)y}]_{mn} = \int \int_{-\infty}^{+\infty} \psi_{2a+m}(x) \psi_{2b+n}(y) \frac{\partial}{\partial y} \left[\psi_{2c+m}(x) \psi_{2d+n}(y) \frac{\partial \ln \epsilon}{\partial x} \right] dx dy. \quad (10.f)$$

When substituting the decomposition Eq. (4) into Eq. (10), the overlap integrals can be calculated analytically with the orthonormality of the Hermite–Gaussian basis functions and the standard integration by parts technique combined with some of the definite integrals available in collections. All of the overlap integrals are not shown here because of their complicated form, which have been discussed in our previous works [23,24].

Through the subscript transform, L_{mn} and \mathcal{E} can be transferred into a $[2 \times F^2] \times [2 \times F^2]$ 2-D matrix and a vector with $2 \times F^2$ elements, with which the eigen system Eq. (9) can be solved directly, the modes and the corresponding propagation constant β can be calculated. There are $2 \times F^2$ eigenvalue- eigenvector pairs for every ‘mn’, so the total results must be $4 \times 2 \times F^2$ eigenvalue- eigenvector pairs after solving eigen equations corresponding to 4 different ‘mn’. When the eigen values at the wavelength λ are labeled in the decreasing order, the electric fields of the modes from the fundamental to higher-order can be obtained.

If the property of the opposite-parity of the electric field is not considered in the algorithm, the decomposition of the transverse electric field cannot be divided into 4 different pairs. Plenty of modes with or without any physically relevant quantities will mix together to make the computations verbose. In order to get $4 \times 2 \times F^2$ eigenvalue- eigenvector pairs, the decomposition terms must be $2F$, and the eigen equation will be a $[2 \times (2F)^2] \times [2 \times (2F)^2]$ 2-D matrix in which the element number exhibits an increase factor of $4 \times 4 = 16$ than that discussed above. The computation time is mainly dominated by three mechanisms: (1) constructing the matrix by analytically calculating definite integrals of Hermite–Gaussian functions, (2) the localization property of the Hermite–Gaussian functions increasing the efficiency and the accuracy for the confined modes and (3) the eigen systems with much less matrix elements greatly reducing the computation time for solving eigenvalue problems when standard algorithms are employed.

All information of the transverse electric field is included in the eigen equation (9). The vector property is reflected by both x - and y - components; the coupling property is included in

the coupled terms $I^{(4)x}$ and $I^{(4)y}$; the fiber with complex dielectric structure can be investigated while it is made of the dielectric constant with negative or positive imaginary part (gain or absorption); the degeneracy property can be obtained from the full vectorial coupling wave equation.

4. Numerical results

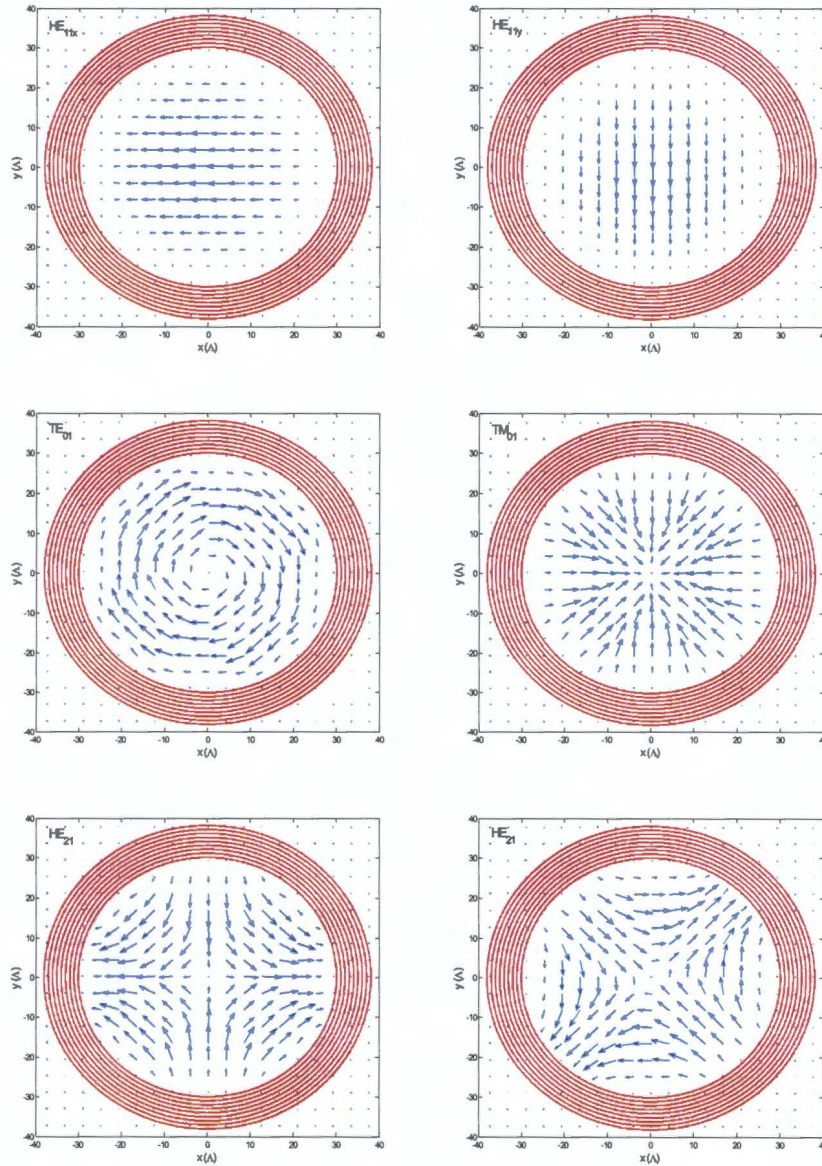


Fig. 3. The electric field of the modes HE_{11} , TE_{01} , TM_{01} and HE_{21} of the Bragg fiber with the structure parameters same as in Fig. 2, the annular dielectric constant is superimposed.

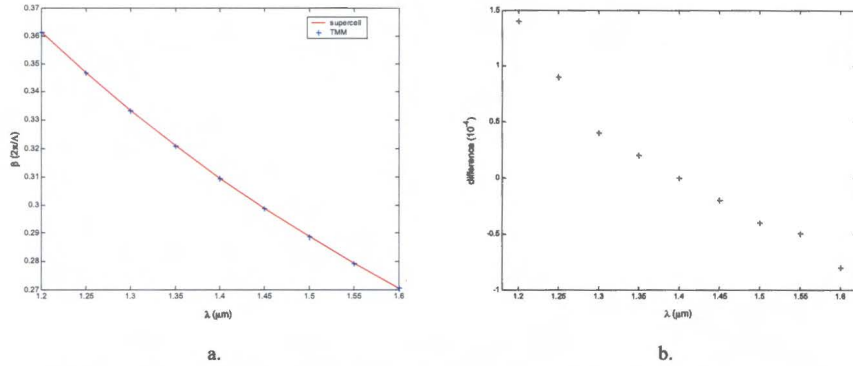


Fig. 4. (a) The propagation constant of TE_{01} mode, and (b) the difference between two different approaches

The mode characteristics of the Bragg fiber are obtained by numerical computations in which the parameter F is set as 15. The transverse electric field of the lowest-order mode, which is a degenerated pair of modes HE_{11x} and HE_{11y} , and the second order modes are quivered in Fig. 3 at wavelength 1550nm. It can be found that light is strongly confined in the low index air core by the PBG due to the outside annular Bragg reflector. The critical property of TE_{0m} (especially TE_{01}) modes is that they have a node in their electric field (E_ϕ) near $r=R$. The fractional $|E|^2$ in the cladding, hence the radiation loss, scales as $1/R^3$ and $1/R$ for TE_{0m} and other modes (TM, HE, EH), respectively. Because of the substantial discrimination between the single lowest-loss mode TE_{01} and other higher-order guided modes, it allows even a highly multimode omniguide fiber to operate in an effectively single-mode fashion [9,11].

The propagation constant of mode TE_{01} is shown in Fig. 4(a), in which the solid line is obtained by the supercell method, and the cross is computed by the transfer matrix method (TMM). The difference between both approaches is demonstrated in Fig. 4(b). In our computation for the case with $A=0.434\mu\text{m}$, $\lambda=1550\text{nm}$, i.e. $\omega=0.28\times 2\pi c/A$, which is same as Ref. [11], the propagation constant is $0.2792093\times 2\pi/A$, which has very good agreement with the value $\beta=0.27926\times 2\pi/A$ in Ref. [11]. It shows the reliability of our model.

5. Conclusion

A compact supercell method based on the opposite parity of the transverse electric field for the Bragg fibers is proposed to investigate the modal properties in this paper. The modal electric field is expanded as the sum of the orthonormal set of Hermite-Gaussian basis functions, a square lattice is constructed by the whole transverse profile of the Bragg fiber which is considered as a supercell, and the periodical dielectric structure of the square lattice is decomposed using periodic functions (cosine). Considering the function relations and the orthonormality of Hermite-Gaussian functions, the propagation characteristics of Bragg fibers are obtained after recasting the full vectorial coupling wave equation into an eigenvalue system. Since the expansion of the transverse electric field is complete and compact due to the opposite parity in the even-parity dielectric waveguide, and all the decomposition coefficients and the overlap integrals are evaluated analytically, this model is efficient and accurate. This method is implemented with very high efficiency and agreement with some literatures [11,17].